Theory of ballistic quantum transport in the presence of localized defects

K. Kolasiński, A. Mreńca-Kolasińska, and B. Szafran
AGH University of Science and Technology, Faculty of Physics and Applied Computer Science, al. Mickiewicza 30, 30-059 Kraków, Poland
(Received 1 July 2016; published 2 September 2016)

We present an efficient numerical approach for treating ballistic quantum transport across devices described by tight-binding (TB) Hamiltonians designated to systems with localized potential defects. The method is based on the wave function matching approach, Lippmann-Schwinger equation (LEQ), and the scattering matrix formalism. We show that the number of matrix elements of the Green's function to be evaluated for the unperturbed system can be essentially reduced by projection of the time reversed scattering wave functions on LEQ which radically improves the speed and lowers the memory consumption of the calculations. Our approach can be applied to quantum devices of an arbitrary geometry and any number of degrees of freedom or leads attached. We provide a couple of examples of possible applications of the theory, including current equilibration at the *p*-*n* junction in graphene and scanning gate microscopy mapping of electron trajectories in the magnetic focusing experiment on a graphene ribbon. Additionally, we provide a simple toy example of electron transport through 1D wire with added onsite perturbation and obtain a simple formula for conductance showing that Green's function of the device can be obtained from the conductance versus impurity strength characteristics.

DOI: 10.1103/PhysRevB.94.115406

I. INTRODUCTION

According to the Landauer approach, the phase coherent component of conductance in nanoscale and mesoscopic systems is determined by quantum scattering of the electron incident from an input channel [1]. The coherent transport problem is of a nonlocal nature, as it is determined by the electron wave function that is defined within the entire device with boundary conditions that are set at the ends of the sample. Nevertheless, in a number of problems, the response of the wave function to a local short-range perturbation is of a central interest for characterization of the sample and its electrical properties. To name a few examples, this is in particular the case for short-range perturbations introduced by the scanning techniques with a probe sweeping the surface of the sample [2–8], for the scattering defects leading to the weak localization [9] and weak antilocalization effects [10–12], or for lattice defects leading to valley mixing in graphene [13]. Moreover, averaging over the coherent scatterers positions is one of the numerical techniques to account for the decoherence effects [14], equilibration of the currents in *n*-*p*-*n* junctions in graphene [15], or investigation of Anderson localization in graphene nanoribbons by introducing the disorder on ribbon edge [16].

Due to a nonlocality of quantum scattering the conductance response of the system to a local perturbation calls for solution of the scattering problem in the entire integration domain. For systems, in which the perturbation can be separated from the Hamiltonian $\tilde{\boldsymbol{H}} = \boldsymbol{H} + \boldsymbol{V}$, one of the available procedures for finding the perturbed wave function is a solution of the Lippman-Schwinger equation [17] spanned by the solution of the transport problem for $\boldsymbol{H}$, the accompanied retarded Green's function, and the perturbation operator $\boldsymbol{V}$. In practice for electron transport problems the Lippman-Schwinger equation is usually treated with the perturbation expansion [18,19] or with iterative schemes [20,21]. In this paper we present a method for an exact solution of the scattering problem with the Lippman-Schwinger equation that requires evaluation of reduced Green's function matrix elements defined within the region affected by the potential perturbation only. The reduction is possible by projection of the Lippman-Schwinger equation on the transport solutions with reversed time flow. The present approach allows for a radical speed-up of the calculations whenever various distributions of the perturbations $\boldsymbol{V}$ for the same Hamiltonian $\boldsymbol{H}$ are needed. For illustration of the method we present applications to scanning gate microscopy of magnetic focusing [22] in graphene [23,24], and for evaluation of the fractional conductance plateaux for graphene *p*-*n* junctions [15,25,26] in the quantum Hall regime [27,28].

The paper is organized as follows. In the next section we recall some basics and introduce necessary quantities needed for the quantum scattering problem described within the robust and commonly used wave function matching method [29–31]. In Sec. III we recall the tight-binding version of the Lippmann-Schwinger equation. Next we show that by projecting the time reversed scattering wave functions on the Lippmann-Schwinger equation we can significantly reduce the number of required Green's functions elements, radically improving the memory consumption and the speed of the algorithm. Later we discuss two examples of application of derived formulas. In Sec. IV we overview the established methods for calculations of the Green's function of unperturbed systems, starting from knitting algorithm for arbitrary shaped devices, fast recursive equations for bulk materials, or modular approach for creating structures. In the last section we show the examples of application of our method for graphene based devices.

II. THE SCATTERING APPROACH FOR UNPERTURBED HAMILTONIAN

We start by describing the wave-function matching approach [29,30,32,33] for solving the scattering problem of arbitrary devices that we use to solve the unperturbed problem for operator H and that provides the elements to define the method for treatment of the local perturbations. We assume that the system of interest can be expressed in terms of finite size matrices like those generated by tight-binding (TB) problems or finite difference approaches. The whole device

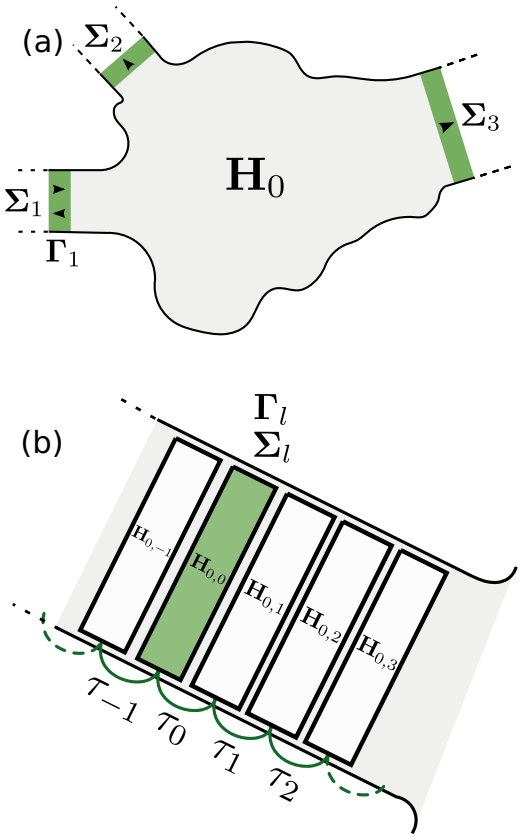

FIG. 1. (a) A sketch of a quantum scatterer described by $\mathbf{H}_0$ coupled to the three semi-infinite leads by self-energy matrices Σ_l. The electron comes from the source represented by Γ_l source vector. The arrows point the possible direction of the scattering electron for this specific example. (b) Block tridiagonal partitioning of the Hamiltonian near the leads from which Σ_l and Γ_l can be computed. The green area denotes the first slice which belongs to the isolated system—the semi-infinite lead and quantum device interface atoms.

can be divided into two parts: the Hamiltonian of isolated system $\boldsymbol{H}_0$ and the self-energy $\boldsymbol{\Sigma}$ term which describes the coupling of the isolated system to the semi-infinite channels [see Fig. 1(a)]. The total Hamiltonian is then defined as

$$\boldsymbol{H} = \boldsymbol{H}_0 + \boldsymbol{\Sigma},$$

where the self-energy matrix contains the contribution from all the leads connected to the device $\boldsymbol{\Sigma} = \boldsymbol{\Sigma}_1 + \cdots + \boldsymbol{\Sigma}_N$.

In order to compute the self-energy matrix $\boldsymbol{\Sigma}_l$ for each lead l one slices the Hamiltonian $\boldsymbol{H}_0$ at the lead interface into the block tridiagonal form [see Fig. 1(b)]

$$-\boldsymbol{\tau}_i \boldsymbol{c}_{i-1} + (E_\mathrm{F} - \boldsymbol{H}_{0,i})\boldsymbol{c}_i - \boldsymbol{\tau}_{i+1}^\dagger \boldsymbol{c}_{i+1} = \boldsymbol{0}, \tag{1}$$

where i enumerates the ith slice from the lead interface ($i = 0$) and $\boldsymbol{\tau}_i$ is the coupling matrix between two consecutive Hamiltonian slices $\boldsymbol{H}_{0,i}$ and $\boldsymbol{H}_{0,i+1}$, and vector $\boldsymbol{c}_i$ is the wave function at slice i.

In this paper we restrict our discussion to the linear transport regime for a small source-drain bias [1], at which the currents are carried by the electrons at the Fermi level E_F which is common for both leads. A more general approach (i.e., nonzero bias) requires integration of the transmission probabilities over the energy window defined by the chemical potentials of the source and drain electrodes [1].

Assuming that the lead is homogeneous, i.e., the Hamiltonian and the coupling matrices do not depend on the position i inside the lead, we may drop the indices in Eq. (1) and obtain the formula

$$-\boldsymbol{\tau}\boldsymbol{c}_{i-1} + (E_\mathrm{F} - \boldsymbol{H}_0)\boldsymbol{c}_i - \boldsymbol{\tau}^\dagger \boldsymbol{c}_{i+1} = \boldsymbol{0}, \tag{2}$$

which can be solved numerically by applying Bloch substitution $\boldsymbol{c}_i = \lambda^i \boldsymbol{u}$ [30,34], where $\lambda^n \equiv e^{ikn}$ describes the plane wave propagation in the channel with k being a wave vector and $\boldsymbol{u}$ a Bloch mode which spans the unit cell. The solution of Eq. (2) leads to the set of eigenpairs $(\{\lambda_1,\boldsymbol{u}_1\},\{\lambda_2,\boldsymbol{u}_2\},\ldots,\{\lambda_{2N_L},\boldsymbol{u}_{2N_L}\})$, where N_L is the length of the $\boldsymbol{c}_i$ vector. Then we group $\{\lambda_i,\boldsymbol{u}_i\}$ into N_L incoming $\{\lambda_{m,+},\boldsymbol{u}_{m,+}\}$ or N_L outgoing $\{\lambda_{m,-},\boldsymbol{u}_{m,-}\}$ modes. Each propagating mode $\boldsymbol{u}_{m,\pm}$ (i.e., with $|\lambda_{m,\pm}| = 1$) is then normalized to carry the unit value of quantum flux [30,34]. We define incoming/outgoing modes matrices as

$$\mathbf{U}_\pm = (\boldsymbol{u}_{1,\pm},\ldots,\boldsymbol{u}_{N_L,\pm})$$

and diagonal $\Lambda_\pm$ matrix constructed from Bloch factors

$$\Lambda_\pm = \begin{pmatrix} \lambda_{1,\pm} & & 0 \\ & \ddots & \\ 0 & & \lambda_{N_L,\pm} \end{pmatrix}.$$

Then the incoming/outgoing Bloch matrices are defined as

$$\mathbf{F}_\pm \equiv \mathbf{U}_\pm \Lambda_\pm^{-1} \mathbf{U}_\pm^{-1}. \tag{3}$$

Description of numerically stable algorithm for calculation of possibly ill-conditioned $F_\pm$ can be found in Ref. [35]. Another approach which involves singular value decomposition (SVD) is explained in Ref. [34]. The self-energy matrix Σ of a given lead l is defined as

$$\Sigma_l \equiv \tau \mathbf{F}_{l,-}.$$

A general expression for the scattering problem can be written in terms of a large but sparse system of linear equations

$$(E_\mathrm{F}\mathbf{1} - \boldsymbol{H})\boldsymbol{\Psi}_{l,m} = \boldsymbol{\Gamma}_{l,m}, \tag{4}$$

where $\Psi_{l,m}$ is the scattering wave function of electron incoming from lead l in mode m and $\boldsymbol{H} = \boldsymbol{H}_0 + \boldsymbol{\Sigma}$. The source vector $\boldsymbol{\Gamma}_{l,m}$ is nonzero only at sites which belong to the lead l, and it is defined as

$$\boldsymbol{\Gamma}_{l,m} = \boldsymbol{\tau}_l(\boldsymbol{F}_{l+} - \boldsymbol{F}_{l-})\,|\boldsymbol{u}_{l,m,+}\rangle\,. \tag{5}$$

After solution of the scattering problem (4) for a given mth incoming mode one may calculate transmission amplitudes through other leads from

$$\boldsymbol{t}_{l,m}^{l'} = \boldsymbol{U}_{l',-}^{-1}\boldsymbol{\Psi}_{l,m}^{L'}, \tag{6}$$

and reflection amplitudes as

$$\boldsymbol{r}_{l,m}^{l} = \boldsymbol{U}_{l,-}^{-1}\left(\boldsymbol{\Psi}_{l,m}^{L} - \boldsymbol{u}_{l,m,+}\right), \tag{7}$$

with $\boldsymbol{U}_{l,-}$ and $\boldsymbol{U}_{l',-}$ being the outgoing modes matrices for input lead l and output leads l', respectively [30]. The

superscripts L', L written by uppercase letters denote the set of elements of vector $\boldsymbol{\Psi}_{l,m}$ which belong to the leads l' or l, respectively. We define $t^{l',m'}_{l,m}/r^{l',m'}_{l,m}$ as the transmission/reflection amplitude that the electron entering the device at lead l in mode m will leave the system at lead l' in mode m'. The transmission/reflection vectors are denoted as $\boldsymbol{t}^{l'}_{l,m}$ and $\boldsymbol{r}^{l'}_{l,m}$, respectively. Having computed $\boldsymbol{t}$ and $\boldsymbol{r}$ amplitudes one calculates transport properties of the system: the electrical conductance, the shot noise, or thermoelectric coefficients. For instance the differential conductance g at temperature 0 K can be computed from the Landauer-Büttiker formula

$$g^{l'}_{l} = \frac{e^2}{h}\sum_{m,m'} \left|t^{l',m'}_{l,m}\right|^2, \tag{8}$$

where the sum over m and m' runs only through propagating modes in lead l and l'.

III. THE TRANSPORT WITH LOCALIZED DISORDER

A. The disorder matrix

We are looking for a solution of the scattering problem of a system distorted by some potential energy operator $\boldsymbol{V}$

$$\tilde{\boldsymbol{H}} = \boldsymbol{H} + \boldsymbol{V}, \tag{9}$$

where we assume that $\boldsymbol{V}$ has the following properties:

(1) $\boldsymbol{V}$ affects only a fraction of sites (and orbitals) P of the whole Hamiltonian $\boldsymbol{H}$, i.e., $|V_{p,q}| \neq 0$ for $p,q \in P$. The performance and memory consumption of the numerical method derived below highly depends on the cardinal number of the P set and will be discussed later. We denote by $\boldsymbol{V}_{PP}$ reduced $\boldsymbol{V}$ matrix of size $N_P = n(P)$ defined as $[\boldsymbol{V}_{PP}]_{p,q} = V_{m(p),m(q)}$, where m($p$) is a function which maps from the local indices of $\boldsymbol{V}_{PP}$ matrix, i.e., from $p,q \in \{1,2,\ldots,N_P\}$ to global indices $m(p),m(q) \in P$ of larger $\boldsymbol{V}$ matrix.

(2) In general $\boldsymbol{V}_{PP}$ can be dense, complex but must be Hermitian ($\boldsymbol{V} = \boldsymbol{V}^\dagger$) in order to conserve the current in the system. Note that the diagonal elements of the potential matrix correspond to the on-site electrostatic potential energy, where the off-diagonal elements correspond to hopping energies between different sites.

(3) $\boldsymbol{V}$ does not affect the sites belonging to the leads, i.e., $\boldsymbol{V}$ does not change the modes in the leads.

B. Lippmann-Schwinger equation

In this section we specify the Lippmann-Schwinger equation for scattering processes and discuss its possible application for TB systems [36]. The perturbed scattering wave function $\tilde{\boldsymbol{\Psi}}_{l,m}$ for the system described with Eq. (9) satisfies scattering equation (4)

$$(E_{\mathrm{F}}\mathbf{1} - \tilde{\boldsymbol{H}})\tilde{\boldsymbol{\Psi}}_{l,m} = \boldsymbol{\Gamma}_{l,m}. \tag{10}$$

Note that the source vector $\boldsymbol{\Gamma}_{l,m}$ does not change, which results from the property (3) of the potential matrix $\boldsymbol{V}$. Without loss of generality we express the new scattering wave function in terms of the unperturbed one

$$\tilde{\boldsymbol{\Psi}}_{l,m} = \boldsymbol{\Psi}_{l,m} + \delta\boldsymbol{\Psi}_{l,m},$$

then using Eqs. (4) and (10) we get

$$\begin{aligned}(E_{\mathrm{F}}\mathbf{1} - (\boldsymbol{H}+\boldsymbol{V}))(\boldsymbol{\Psi}_{l,m} + \delta\boldsymbol{\Psi}_{l,m}) &= \boldsymbol{\Gamma}_{l,m},\\ (E_{\mathrm{F}}\mathbf{1} - \boldsymbol{H})\delta\boldsymbol{\Psi}_{l,m} &= \boldsymbol{V}(\boldsymbol{\Psi}_{l,m} + \delta\boldsymbol{\Psi}_{l,m}).\end{aligned} \tag{11}$$

We define $\boldsymbol{G} = (E_{\mathrm{F}}\mathbf{1} - \boldsymbol{H})^{-1}$ as the Green's function of the unperturbed system. By multiplying Eq. (11) from the left by $\boldsymbol{G}$ we obtain the Lippmann-Schwinger equation for $\delta\boldsymbol{\Psi}_{\mathrm{l,m}}$

$$\delta\boldsymbol{\Psi}_{l,m} = \boldsymbol{G}\boldsymbol{V}(\boldsymbol{\Psi}_{l,m} + \delta\boldsymbol{\Psi}_{l,m}). \tag{12}$$

In order to compute the conductance $g^{l'}_{l}$ [see Eqs. (6) and (8)] of the system with $\boldsymbol{V}$ one has to evaluate the values of $\tilde{\boldsymbol{\Psi}}_{\mathrm{l,m}}$ at each lead l' interface, i.e., vectors $\tilde{\boldsymbol{\Psi}}^{L'}_{l,m}$, thus we only need to compute the elements of the $\delta\Psi_{l,m}$ vector which belong to the given lead. The change in the wave function at site l' is given by

$$\delta\Psi^{l'}_{l,m} = \sum_{p,q} G_{l',p}V_{p,q}\left(\Psi^{q}_{l,m} + \delta\Psi^{q}_{l,m}\right).$$

Using the first property of the V matrix we get

$$\delta\Psi^{l'}_{l,m} = \sum_{p,q\in P} G_{l',p}V_{p,q}\left(\Psi^{q}_{l,m} + \delta\Psi^{q}_{l,m}\right)$$

which in the matrix notation can be written as

$$\delta\boldsymbol{\Psi}^{L'}_{l,m} = \boldsymbol{G}_{L'P}\boldsymbol{V}_{PP}\left(\boldsymbol{\Psi}^{P}_{l,m} + \delta\boldsymbol{\Psi}^{P}_{l,m}\right), \tag{13}$$

where $\boldsymbol{G}_{L'P}$ is the reduced Green's matrix which couples the elements of the lead l' with the perturbed sites P. Similarly, using Eq. (12) we calculate $\delta\boldsymbol{\Psi}^{P}_{l,m}$ as

$$\begin{aligned}\delta\boldsymbol{\Psi}^{P}_{l,m} &= \boldsymbol{G}_{PP}\boldsymbol{V}_{PP}\left(\boldsymbol{\Psi}^{P}_{l,m} + \delta\boldsymbol{\Psi}^{P}_{l,m}\right)\\ &= (1 - \boldsymbol{G}_{PP}\boldsymbol{V}_{PP})^{-1}\boldsymbol{G}_{PP}\boldsymbol{V}_{PP}\boldsymbol{\Psi}^{P}_{l,m},\end{aligned}$$

which substituted to Eq. (13) gives the final formula for the change in the wave function

$$\begin{aligned}\delta\boldsymbol{\Psi}^{L'}_{l,m} &= \boldsymbol{G}_{L'P}\boldsymbol{V}_{PP}(\mathbf{1} + (1 - \boldsymbol{G}_{PP}\boldsymbol{V}_{PP})^{-1}\boldsymbol{G}_{PP}\boldsymbol{V}_{PP})\boldsymbol{\Psi}^{P}_{l,m},\\ &= \boldsymbol{G}_{L'P}\boldsymbol{V}_{PP}(1 - \boldsymbol{G}_{PP}\boldsymbol{V}_{PP})^{-1}\boldsymbol{\Psi}^{P}_{l,m}\\ &\equiv \boldsymbol{G}_{L'P}\boldsymbol{T}_{PP}\boldsymbol{\Psi}^{P}_{l,m},\end{aligned} \tag{14}$$

where

$$\boldsymbol{T}_{PP} = \boldsymbol{V}_{PP}(1 - \boldsymbol{G}_{PP}\boldsymbol{V}_{PP})^{-1} \tag{15}$$

is the transition matrix. Then the transmission probability through lead l' can be computed from Eq. (6)

$$\tilde{\boldsymbol{t}}^{l'}_{l,m} = \boldsymbol{U}^{-1}_{l',-}\left(\boldsymbol{\Psi}^{L'}_{l,m} + \delta\boldsymbol{\Psi}^{L'}_{l,m}\right).$$

Before we proceed to further simplification of Eq. (14), let us discuss some of the numerical properties of the obtained result. Firstly, in order to find the transmission probabilities one has to compute the selected elements of the Green's function of unperturbed system $\boldsymbol{G}$, which are needed to construct two reduced matrices: $\boldsymbol{G}_{L'P}$ and $\boldsymbol{G}_{PP}$. We will discuss this problem in the next sections, but for now we assume that those matrices can be computed with available algorithms. Secondly, having $\boldsymbol{G}_{L'P}$ and $\boldsymbol{G}_{PP}$ one may compute conductance without solving a large system of linear equations (4) which allows for speed up of the calculations. The speed of the algorithm will depend on the computational time C_{P} needed to calculate

the $\boldsymbol{G}_{L'P}\boldsymbol{T}_{PP}$ matrix, time C_{G} needed for calculation of the reduced Green's functions, and time C_{W} needed for calculation of the unperturbed wave functions. On the other hand the computation time for the standard method is only C_{W} since the perturbation matrix $\mathbf{V}$ does not change the solution time of Eq. (10). Hence, for a single scattering process the proposed method is slower by ratio $(C_{\mathrm{P}}+C_{\mathrm{G}}+C_{\mathrm{W}})/C_{\mathrm{W}}$. However, when one is interested in statistical properties of current and needs to compute conductance N times for different $\boldsymbol{V}_{PP}$ matrices (here we assume that the set of perturbed sites P does not change, i.e., we can compute $\boldsymbol{G}_{L'P}$ and $\boldsymbol{G}_{PP}$ once and store them in memory) the ratio becomes $(NC_{\mathrm{P}}+C_{\mathrm{G}}+C_{\mathrm{W}})/(NC_{\mathrm{W}})$ and for $N\to\infty$ leads to $C_{\mathrm{P}}/C_{\mathrm{W}}$, which in general can be an arbitrarily small number. Note that the time C_{P} depends only on the size of the $\boldsymbol{V}_{PP}$ matrix, which means that for small V_{PP}, i.e., $\leqslant$1000 finding the transmission amplitudes for a system with 10^6 sites may be significantly reduced from minutes to fraction of seconds. Finally, the form of Eq. (14) requires allocation of several dense matrices, two of size $N_P\times N_P$ ($\boldsymbol{G}_{PP}$ and $\boldsymbol{V}_{PP}$) and L matrices of size $N_{L'}\times N_P$ ($\boldsymbol{G}_{L'P}$), where $N_{L'}$ is the total number of elements in the lead l' vector and L is the total number of leads in the system. The value of N_P can be controlled by choosing the number of disordered sites in the system, however the $N_{L'}$ depends on the device structure and can be in general very large increasing the memory usage and the times C_{G}, C_{P}. We propose then to use Eq. (14) as a starting point for a more complicated approach discussed in the next paragraph.

C. Excluding the $G_{L'P}$ terms

In this section we show that the $\boldsymbol{G}_{L'P}$ term can be eliminated from Eq. (14). Firstly, let us note that another matrix $\boldsymbol{G}_{PL'}$ can be related with the scattering wave function at the sites P with equation

$$\boldsymbol{\Psi}^{P}_{l,m}=\boldsymbol{G}_{PL}\boldsymbol{\Gamma}^{L}_{l,m},$$

where we used Eq. (4) and the sparsity of the source vector, i.e., $\boldsymbol{\Gamma}^{Q}_{l,m}=0$ for $Q\notin L$. Now, we look for a similar relation for $\boldsymbol{G}_{L'P}$. Firstly, we note that by conjugating Hamiltonian $\boldsymbol{H}_0\to\boldsymbol{H}_0^{*}=\boldsymbol{H}_0^{T}$ in Eq. (4) we obtain a scattering problem for the particle propagating backward in time

$$\overleftarrow{\boldsymbol{\Psi}}_{l',n}=\overleftarrow{\boldsymbol{G}}\,\overleftarrow{\boldsymbol{\Gamma}}_{l',n}, \tag{16}$$

where the symbol $\overleftarrow{X}\equiv X[\boldsymbol{H}_0^{*}]$ denotes that variable X is computed as usual but for conjugated Hamiltonian matrix $\boldsymbol{H}_0^{*}$, $\overleftarrow{\boldsymbol{\Psi}}_{l',n}$ and $\overleftarrow{\boldsymbol{\Gamma}}_{l',n}$ are the column vectors, and the Green's function $\overleftarrow{\boldsymbol{G}}$ is calculated as

$$\overleftarrow{\boldsymbol{G}}=\frac{1}{E_{\mathrm{F}}\mathbf{1}-(\boldsymbol{H}_0^{*}+\overleftarrow{\boldsymbol{\Sigma}})}.$$

Additionally, since $\boldsymbol{H}_0^{*}=\boldsymbol{H}_0^{T}$ one may prove that $\overleftarrow{\boldsymbol{\Sigma}}=\boldsymbol{\Sigma}^{T}$ which leads to the following identity $\overleftarrow{\boldsymbol{G}}^{T}=\boldsymbol{G}$. Using this relation and transposing Eq. (16) we may write

$$\overleftarrow{\boldsymbol{\Psi}}^{(T)}_{l',n}=\overleftarrow{\boldsymbol{\Gamma}}^{(T)}_{l',n}\overleftarrow{\boldsymbol{G}}^{T}=\overleftarrow{\boldsymbol{\Gamma}}^{(T)}_{l',n}\boldsymbol{G},$$

where for clarity we denote transposition as (T) in order to distinguish it from other superscripts. Evaluating this expression at sites belonging to P set we get

$$\overleftarrow{\boldsymbol{\Psi}}^{P(T)}_{l',n}=\overleftarrow{\boldsymbol{\Gamma}}^{L'(T)}_{l',n}\boldsymbol{G}_{L'P}. \tag{17}$$

Let us now project the $\overleftarrow{\boldsymbol{\Gamma}}^{L'(T)}_{l',n}$ vectors on the scattering wave function at lead l' [see Eq. (14)]

$$\tilde{\boldsymbol{\Psi}}^{L'}_{l,m}-\boldsymbol{\Psi}^{L'}_{l,m}=\boldsymbol{G}_{L'P}\boldsymbol{T}_{PP}\boldsymbol{\Psi}^{P}_{l,m}.$$

Using Eq. (17) we get

$$\overleftarrow{\boldsymbol{\Gamma}}^{L'(T)}_{l',n}\big(\tilde{\boldsymbol{\Psi}}^{L'}_{l,m}-\boldsymbol{\Psi}^{L'}_{l,m}\big)=\overleftarrow{\boldsymbol{\Psi}}^{P(T)}_{l',n}\boldsymbol{T}_{PP}\boldsymbol{\Psi}^{P}_{l,m}.$$

The equation above can be related with transmission probabilities (6)

$$\overleftarrow{\boldsymbol{\Gamma}}^{L'(T)}_{l',n}\boldsymbol{U}_{l',-}\delta\boldsymbol{t}^{l'}_{l,m}=S^{l',n}_{l,m}, \tag{18}$$

where we define the elements of the scattering overlap matrix $\boldsymbol{S}^{l'}_{l,m}$

$$S^{l',n}_{l,m}\equiv\overleftarrow{\boldsymbol{\Psi}}^{P(T)}_{l',n}\boldsymbol{T}_{PP}\boldsymbol{\Psi}^{P}_{l,m}$$

and the variation in the transmission vector

$$\delta\boldsymbol{t}^{l'}_{l,m}\equiv\tilde{\boldsymbol{t}}^{l'}_{l,m}-\boldsymbol{t}^{l'}_{l,m}=\boldsymbol{U}^{-1}_{l',-}\big(\tilde{\boldsymbol{\Psi}}^{L'}_{l,m}-\boldsymbol{\Psi}^{L'}_{l,m}\big). \tag{19}$$

Let us now discuss the dimensions of the vectors and matrices present in the equations above. The $\boldsymbol{\Psi}^{P}_{l,m}$ is a column vector of length N_P. We define a matrix

$$\boldsymbol{\Psi}^{P}_{M_L}\equiv\big(\boldsymbol{\Psi}^{P}_{l,1},\boldsymbol{\Psi}^{P}_{l,2},\ldots,\boldsymbol{\Psi}^{P}_{l,M_L}\big), \tag{20}$$

composed from vectors $\boldsymbol{\Psi}^{P}_{l,m}$, where the uppercase subscript M_L denotes the number of propagating modes in lead l at given E_{F}. Hence $\boldsymbol{\Psi}^{P}_{M_L}$ is a rectangular matrix of size $N_P\times M_L$. Similarly, for the rest of the leads l', we define

$$\overleftarrow{\boldsymbol{\Psi}}^{P(T)}_{M_{L'}}\equiv\big(\overleftarrow{\boldsymbol{\Psi}}^{P}_{l',1},\overleftarrow{\boldsymbol{\Psi}}^{P}_{l',2},\ldots,\overleftarrow{\boldsymbol{\Psi}}^{P}_{l',M_{L'}}\big)^{T} \tag{21}$$

being a matrix of size $M_{L'}\times N_P$. Let us now define a source matrix for modes propagating from lead l' backward in time

$$\overleftarrow{\boldsymbol{\Gamma}}^{L'(T)}_{M_{L'}}\equiv\big(\overleftarrow{\boldsymbol{\Gamma}}^{L'}_{l',1},\overleftarrow{\boldsymbol{\Gamma}}^{L'}_{l',2},\ldots,\overleftarrow{\boldsymbol{\Gamma}}^{L'}_{l',M_{L'}}\big)^{T}. \tag{22}$$

The size of this matrix is $M_{L'}\times N_{L'}$. Finally, the modes matrices $\boldsymbol{U}_{l',-}$ and the transmission vectors $\tilde{\boldsymbol{t}}^{l'}_{l,m}$ have dimensions $N_{L'}\times N_{L'}$ and $N_{L'}\times 1$, respectively.

Let us note that $\boldsymbol{t}^{l'}_{l,m}$ is a vector which in general can be divided into two parts: (i) scattering amplitudes of propagating modes and (ii) evanescent modes. Despite the fact that the second term does not contribute to the current in the Landauer formula the coefficients are usually nonzero and play an important role for construction of the open boundary conditions at leads interfaces. The structure of the $\boldsymbol{t}$ vector can be written in general form

$$\boldsymbol{t}^{l'}_{l,m}=\big(t^{l',1}_{l,m},\ldots,t^{l',M_{L'}}_{l,m},t^{l',M_{L'}+1}_{l,m},\ldots,t^{l',N_{L'}}_{l,m}\big)^{T},$$

with $t^{l',M_{L'}+1}_{l,m},\ldots,t^{l',N_{L'}}_{l,m}$ being the amplitudes of evanescent modes. In the following we assume that the disorder introduced by $\boldsymbol{V}_{PP}$ matrix does not affect the evanescent modes at each lead. From the above assumption the change in the scattering

amplitudes affects the transport modes only

$$\delta \boldsymbol{t}^{l'}_{l,m} = \left(\delta t^{l',1}_{l,m}, \ldots, \delta t^{l',M_{L'}}_{l,m}, 0, \ldots, 0\right)^T, \tag{23}$$

$$\equiv \left(\delta \tilde{\boldsymbol{t}}^{l'}_{l,m}, \mathbf{0}_{1\times N_{L'}-M_{L'}}\right)^T, \tag{24}$$

which shows that we can truncate the last $N_{L'} - M_{L'}$ columns of modes matrix $\boldsymbol{U}_{l',-}$ in Eq. (18). Let us note that the assumption that the evanescent mode amplitudes are not affected by the $\boldsymbol{V}_{PP}$ matrix requires that the perturbation is introduced at a sufficient distance from the lead within the scattering region.

Let us then define the truncated matrix $\boldsymbol{U}_{l',-}$ as $\boldsymbol{U}^{\mathrm{trnc}}_{l',-}$ which has dimensions $N_{L'} \times M_{L'}$ and is obtained from the first $M_{L'}$ columns of $\boldsymbol{U}_{l',-}$. Using the definitions above we can write Eq. (19) in the following way

$$\overleftarrow{\boldsymbol{\Gamma}}^{L'(T)}_{M_{L'}} \boldsymbol{U}^{\mathrm{trnc}}_{l',-} \delta \tilde{\boldsymbol{t}}^{l'}_{l,m} = \boldsymbol{S}^{l'}_{l,m},$$

where the product

$$\overleftarrow{\boldsymbol{D}}_{l'} \equiv \overleftarrow{\boldsymbol{\Gamma}}^{L'(T)}_{M_{L'}} \boldsymbol{U}^{\mathrm{trnc}}_{l',-} \tag{25}$$

is now a square matrix of size $M_{L'} \times M_{L'}$. Multiplying the equation above by $\overleftarrow{\boldsymbol{D}}^{-1}_{l'}$ from the left we get

$$\delta \tilde{\boldsymbol{t}}^{l'}_{l,m} = \overleftarrow{\boldsymbol{D}}^{-1}_{l'} \boldsymbol{S}^{l'}_{l,m},$$

from which one may compute transmission probabilities for propagating modes

$$\tilde{\boldsymbol{T}}^{l'}_{l,m} \equiv \left|\tilde{\boldsymbol{t}}^{l'}_{l,m}\right|^2 = \left|\boldsymbol{t}^{l'}_{l,m} + \overleftarrow{\boldsymbol{D}}^{-1}_{l'} \boldsymbol{S}^{l'}_{l,m}\right|^2 \tag{26}$$

and conductance $\tilde{g}^{l'}_{l}$ (8).

In case of the reflection amplitudes $\boldsymbol{r}^{l}_{l,m}$ defined in equation (7) we can write the perturbed ones as

$$\tilde{\boldsymbol{r}}^{l}_{l,m} = \boldsymbol{U}^{-1}_{l,-}\left(\boldsymbol{\Psi}^{L}_{l,m} - \boldsymbol{u}_{l,m,+} + \delta\boldsymbol{\Psi}^{L}_{l,m}\right) \equiv \boldsymbol{r}^{l}_{l,m} + \delta\tilde{\boldsymbol{r}}^{l}_{l,m},$$

with $\delta\tilde{\boldsymbol{r}}^{l}_{l,m} = \boldsymbol{U}^{-1}_{l,-}\delta\boldsymbol{\Psi}^{L}_{l,m}$. Following exactly the same steps as in the case of $\boldsymbol{t}^{l'}_{l,m}$ we obtain $\delta\tilde{\boldsymbol{r}}^{l}_{l,m} = \overleftarrow{\boldsymbol{D}}^{-1}_{l}\boldsymbol{S}^{l}_{l,m}$, which shows that if we redefine $\boldsymbol{r}^{l}_{l,m} \to \boldsymbol{t}^{l}_{l,m}$ then Eq. (26) defines the reflection probabilities when $l' = l$.

D. Numerical algorithm

To conclude the previous section the following algorithm can be used to compute the scattering matrix for system with potential matrix $\boldsymbol{V}$:

(1) Compute and store the following matrices for system without disorder potential [see Eq. (4)]: (a) the scattering wave functions $\boldsymbol{\Psi}_{l,m}$ for selected leads and modes in those leads. (b) the outgoing modes matrices $\boldsymbol{U}_{l',-}$ and $\boldsymbol{t}^{l}_{l,m}$(i.e., scattering matrix).

(2) Compute and store the following matrices for system with $\boldsymbol{H}_0 \to \boldsymbol{H}^*_0$ in Eq. (4). (a) all the scattering wave functions $\overleftarrow{\boldsymbol{\Psi}}_{l',n}$ and (b) source vectors $\overleftarrow{\boldsymbol{\Gamma}}^{L'}_{l',n}$ for time reversed problem.

(3) Compute reduced matrices $\boldsymbol{\Psi}^{P}_{M_L}$ from Eq. (20), $\overleftarrow{\boldsymbol{\Psi}}^{P(T)}_{M_{L'}}$ from Eq. (21), $\overleftarrow{\boldsymbol{\Gamma}}^{L'(T)}_{M_{L'}}$ from Eq. (22), and $\overleftarrow{\boldsymbol{D}}_{l'}$ from Eq. (25).

(4) Calculate the selected elements of the Green's function $\boldsymbol{G}_{PP}$ and reduced disorder matrix $\boldsymbol{V}_{PP}$.

(5) Construct the transition matrix $\boldsymbol{T}_{PP}$ from Eq. (15).

(6) Compute new scattering amplitudes $\tilde{\boldsymbol{t}}^{l'}_{l,m}$ from Eq. (26) from which conductance (8) can be calculated.

E. Discussion

The general relation between the scattering matrix and the transition matrix (26) can be used for any type of scattering problem which can be described by Eq. (4), hence it is relevant for any kind of TB systems or, e.g., Hamiltonians generated by finite difference (or finite elements [32,37]) methods. Then different kinds of forms of $\boldsymbol{V}_{PP}$ can be used to simulate random onsite potential in quantum structures (diagonal form of $\boldsymbol{V}_{PP}$), point defects in the lattice, adatoms [38–40], or modification of existing hoping energies (off-diagonal elements). The advantage of Eq. (26) over the basic Lippmann-Schwinger Eq. (14) is that one reduces the number of Green's function elements to be computed, which for arbitrary systems can be a memory and time consuming task. On the other hand one has to compute all the scattering wave functions for particle propagating backward in time $\overleftarrow{\boldsymbol{\Psi}}_{l',n}$, however this can be done efficiently with existing numerical libraries [41,42]. Additionally, for well written quantum transport solvers this problem reduces to replacing the original Hamiltonian by its conjugation which is a straightforward task. Additionally, in a special case when $\boldsymbol{H}_0$ is real the relation $\overleftarrow{\boldsymbol{X}} = \boldsymbol{X}$ holds, hence one does not have to compute $\overleftarrow{\boldsymbol{\Psi}}_{l',n}$ and other matrices separately.

F. Weak perturbation limit

An interesting case arises when one takes the limit $\boldsymbol{G}_{PP}\boldsymbol{V}_{PP} \to 0$ in Eq. (15), i.e., $\boldsymbol{V}_{PP}$ generates weak perturbation in the Hamiltonian

$$\begin{aligned}\boldsymbol{T}_{PP} &= \boldsymbol{V}_{PP}(1 - \boldsymbol{G}_{PP}\boldsymbol{V}_{PP})^{-1} \approx \boldsymbol{V}_{PP}(1 - \boldsymbol{G}_{PP}\boldsymbol{V}_{PP}) \\ &= \boldsymbol{V}_{PP} - \boldsymbol{V}_{PP}\boldsymbol{G}_{PP}\boldsymbol{V}_{PP}.\end{aligned}$$

In this limit one may compute the correction to the scattering matrix as

$$\begin{aligned}\tilde{\boldsymbol{t}}^{l'}_{l,m} &= \boldsymbol{t}^{l'}_{l,m} + \overleftarrow{\boldsymbol{D}}^{-1}_{l'} \overleftarrow{\boldsymbol{\Psi}}^{P(T)}_{M_{L'}} \boldsymbol{T}_{PP} \boldsymbol{\Psi}^{P}_{M_L} \\ &\approx \boldsymbol{t}^{l'}_{l,m} + \boldsymbol{t}^{l'(1)}_{l,m} + \boldsymbol{t}^{l'(2)}_{l,m},\end{aligned}$$

with the first (1) and the second (2) order corrections being

$$\begin{aligned}\boldsymbol{t}^{l'(1)}_{l,m} &= \overleftarrow{\boldsymbol{D}}^{-1}_{l'} \overleftarrow{\boldsymbol{\Psi}}^{P(T)}_{M_{L'}} \boldsymbol{V}_{PP} \boldsymbol{\Psi}^{P}_{M_L} \\ \boldsymbol{t}^{l'(2)}_{l,m} &= -\overleftarrow{\boldsymbol{D}}^{-1}_{l'} \overleftarrow{\boldsymbol{\Psi}}^{P(T)}_{M_{L'}} \boldsymbol{V}_{PP} \boldsymbol{G}_{PP} \boldsymbol{V}_{PP} \boldsymbol{\Psi}^{P}_{M_L}.\end{aligned} \tag{27}$$

Note that the first correction does not require the information about Green's function. Similar expression for the first order correction (27) to the scattering matrix has been derived recently [18] in the context of scanning gate microscopy technique. The present result generalizes the ones of Ref. [18] to the case of magnetic field, the spin degree of freedom, or any other system that can be described within the single-electron transport problem defined by Eq. (4).

G. 1D case

Let us discuss another example of one-dimensional quantum transport with a single scattering mode in the leads.

We show that for the case when the perturbation potential is localized on one site P (δ-like potential) we can find simple expression for the conductance which relates conductance g with the Green's function at site P.

For this case we can drop all the indices in Eq. (26) and work only with scalar variables

$$\tilde{t} = t + c_P V_P (1 - G_{PP} V_P)^{-1} \tag{28}$$

with $c_P = \overleftarrow{D}^{-1} \overleftarrow{\Psi}^P \Psi^P$ and V_P being the onsite potential affecting site P. For an infinite potential barrier $V_P = +\infty$ the scattered electron will be completely reflected, hence

$$\lim_{V_P \to +\infty} \tilde{t} = 0 = t - c_P G_{PP}^{-1} \Rightarrow t = c_P G_{PP}^{-1}.$$

Using this result we simplify Eq. (28)

$$\tilde{t} = c_P G_{PP}^{-1} + \frac{c_P V_P}{1 - G_{PP} V_P} = \frac{c_P G_{PP}^{-1}}{1 - G_{PP} V_P} = \frac{t}{1 - G_{PP} V_P},$$

from which we can compute the two terminal conductance

$$\tilde{g} = g \frac{1}{1 + [\Re\{G_{PP}\}^2 + \Im\{G_{PP}\}^2] V_P^2 - 2 V_P \Re\{G_{PP}\}}, \tag{29}$$

with g being the conductance of the unperturbed system. From the equation above we see that by adding a localized potential at some point P to the quantum wire we can perform a scan in function of the V_P amplitude and then fit the obtained response $\tilde{g}$ to Eq. (29) in order to obtain the information about the Green's function (real and imaginary part, i.e., LDOS) of the device at point P. Another approach would be to calculate numerically the first and second derivative of $\tilde{g}$ with respect to perturbation strength V_P

$$\frac{1}{g} \frac{d\tilde{g}}{dV_P}\bigg|_{V_P=0} = 2\Re\{G_{PP}\}$$

$$\frac{1}{g} \frac{d^2\tilde{g}}{dV_P^2}\bigg|_{V_P=0} = 6\Re\{G_{PP}\}^2 - 2\Im\{G_{PP}\}^2.$$

Expression (29) is exact for delta-like perturbations, however it should be also valid for finite size potentials when the effective width of perturbation is smaller than half of the Fermi wavelength $d_V \leqslant \lambda_F/2$. One should also note that the Eq. (28) is valid also for any device (2D or 3D) which carries only one transverse mode.

IV. COMPUTING THE GREEN'S FUNCTION

In this section we overview the procedures used for evaluation of the Green's function matrices, for a general case (IV A), for a devices with translational symmetry (IV B), and the combined modular approach for calculation of the Green's function (IV C).

A. Computing selected elements of G for arbitrary devices

One of the most challenging aspects of the derived method is the calculation of selected elements of the Green's function of unperturbed system $\boldsymbol{G} = (E_F \mathbf{1} - \boldsymbol{H})^{-1}$. Since $\boldsymbol{H}$ in usual applications is a large (e.g., $\sim 10^5 - 10^6$) and sparse matrix, its inverse is dense and cannot be computed with direct inversion algorithms. In order to overcome this problem various algorithms were developed to compute only the necessary elements of $\boldsymbol{G}$ instead of a whole matrix. A popular method called recursive Green's function (RGF) which involves the Dyson equation developed in a number of variants is used for this purpose, e.g., see Refs. [43–46]. Unfortunately many of those variants are limited to a specific geometry of device [47] or can be used only for two terminal devices or special slicing has to be performed in order to include the effect of multiterminal devices [48].

However, recently a variation of RGF method has been developed which generalizes the standard approach, leading to numerically stable knitting algorithm [49]. The knitting algorithm can be applied to arbitrary shaped devices with arbitrary number of leads, orbitals, etc. In general the method of Ref. [49] can be used to compute selected elements of the inverse of any structurally symmetric sparse matrix. For more details about implementation, numerical scaling, or memory usage we refer the reader to the original paper [49]. Alternatively one may use the efficient nested dissection approach as described recently in Ref. [50].

To summarize this section, the selected elements of the Green's function $\boldsymbol{G}$ can be computed with available algorithms, but for general purpose it may be practical to implement an universal algorithm from Ref. [49]. For testing purpose we provide the source code of our implementation of the knitting algorithm [51] written in Fortran.

B. Computing G of translational invariant devices

In this section we explain that for a special case of quantum channels with translational symmetry (bulk materials) the general formula for a Green's function can be found for any type of Hamiltonian including the topology, number of orbitals, or dimensionality of the problem [16,31,44].

Let us recall that any translationally invariant quantum channel generated by the TB problems can be described by general block tridiagonal Hamiltonian $E_F \mathbf{1} - \boldsymbol{H}_0$ [30,52] of form

$$-\boldsymbol{H}_{0i,i-1} \boldsymbol{c}_{i-1} + (E_F \mathbf{1} - \boldsymbol{H}_{0i,i}) \boldsymbol{c}_i - \boldsymbol{H}_{0i,i+1} \boldsymbol{c}_{i+1} = \mathbf{0},$$

where $\boldsymbol{c}_i$ describes the wave function at the ith slice, the diagonal block $\boldsymbol{H}_{0,i,i}$ is the Hamiltonian of the isolated slice, and $\boldsymbol{H}_{0i,i-1} = \boldsymbol{H}_{0i,i+1}^{\dagger} = \boldsymbol{\tau}$ represents coupling between slices $i \mp 1$ and i. Assumed translation symmetry requires invariance of block matrices after shift along the diagonal of $\boldsymbol{H}$ matrix

$$\boldsymbol{H}_{0i+k,j+k} = \boldsymbol{H}_{0i,j},$$

then if considered channel is infinite the same property is also satisfied by Green's function $\boldsymbol{G}_0 = (E_F \mathbf{1} - \boldsymbol{H}_0)^{-1}$

$$\boldsymbol{G}_{0i+k,j+k} = \boldsymbol{G}_{0i,j}, \tag{30}$$

which shows that knowledge about $\boldsymbol{G}_{0i,j\pm k}$ is enough to reproduce any blocks of the Green's function. The infinite device can be truncated with self-energies as in Eq. (4),

$$\boldsymbol{\Psi}_{l,m} = (E_F \mathbf{1} - \boldsymbol{H})^{-1} \boldsymbol{\Gamma}_{l,m} = \boldsymbol{G} \boldsymbol{\Gamma}_{l,m}.$$

Let us assume that an electron enters the channel in mode $|\boldsymbol{u}_{m,-}\rangle$, from the left lead $l \equiv L$ [i.e., an electron is injected by

the source vector $\mathbf{\Gamma}_{L,m}$, see Eq. (5)] and at site $i = 0$. Then the scattering wave function at ith slice is given by

$$|\boldsymbol{c}_{i,m}\rangle = \boldsymbol{G}_{i,0}\mathbf{\Gamma}_{L,m} = \boldsymbol{G}_{i,0}\boldsymbol{\tau}_L(\boldsymbol{F}_{L,+} - \boldsymbol{F}_{L,-})\,|\boldsymbol{u}_{L,m,-}\rangle\,. \quad (31)$$

Since the derivation involves only the left lead, we can drop the subscript L in all the equations below. On the other hand we can write the exact formula for the scattering mode at slice i (pure propagation in the bulk)

$$|\boldsymbol{c}_{i,m}\rangle = \lambda_{m,-}^{-i}\,|\boldsymbol{u}_{m,-}\rangle\,. \quad (32)$$

By putting Eqs. (31) and (32) together and using the matrix notation we get

$$\boldsymbol{U}_-\mathbf{\Lambda}_-^{-i} = \boldsymbol{G}_{i,0}\boldsymbol{\tau}(\boldsymbol{F}_+ - \boldsymbol{F}_-)\boldsymbol{U}_-,$$

from which we obtain

$$\begin{aligned}\boldsymbol{G}_{i,0} &= \boldsymbol{U}_-\mathbf{\Lambda}_-^{-i}\boldsymbol{U}_-^{-1}[\boldsymbol{\tau}(\boldsymbol{F}_+ - \boldsymbol{F}_-)]^{-1}\\ &= \boldsymbol{F}_-^{i}[\boldsymbol{\tau}(\boldsymbol{F}_+ - \boldsymbol{F}_-)]^{-1},\end{aligned}$$

where we used Eq. (3). By setting $i = 0$ we obtain a general expression for the diagonal blocks of the Green's matrix

$$\boldsymbol{G}_{k,k} = \boldsymbol{G}_{0,0} = [\boldsymbol{\tau}(\boldsymbol{F}_+ - \boldsymbol{F}_-)]^{-1}, \quad (33)$$

which leads to the recursive formula for right off-diagonal elements $\boldsymbol{G}_{i+k,k}$

$$\boldsymbol{G}_{i+k,k} = \boldsymbol{G}_{i,0} = \boldsymbol{F}_-^{i}\boldsymbol{G}_{0,0} = \boldsymbol{F}_-\boldsymbol{G}_{i-1,0}, \quad \text{for i} \geqslant 1. \quad (34)$$

For the left off-diagonal blocks we get an analogical expression

$$\boldsymbol{G}_{-i,0} = \boldsymbol{G}_{-i+k,k} = \boldsymbol{F}_+^{i}\boldsymbol{G}_{0,0} = \boldsymbol{F}_+\boldsymbol{G}_{-i+1,0}, \quad \text{for i} \geqslant 1. \quad (35)$$

The diagonal block matrix $\boldsymbol{G}_{k,k}$ can be directly computed from Eq. (33). However, this can be numerically unstable since both Bloch matrices $\boldsymbol{F}_\pm$ and the coupling matrix $\boldsymbol{\tau}$ can be in general ill defined [34]. To overcome this problem one may find $\boldsymbol{G}_{k,k}$ by using one of the RGF methods discussed in the previous section. However, we can use the fact that in general $\boldsymbol{G}_{k,k}$ does not depend on the length of the device and the smallest possible device which can be created is 2×2 block matrix

$$\begin{bmatrix}\boldsymbol{G}_{0,0} & \boldsymbol{G}_{0,1}\\ \boldsymbol{G}_{1,0} & \boldsymbol{G}_{1,1}\end{bmatrix} = \begin{bmatrix}E_{\mathrm{F}}\mathbf{1} - (\boldsymbol{h} + \mathbf{\Sigma}_L) & \boldsymbol{\tau}^\dagger\\ \boldsymbol{\tau} & E_{\mathrm{F}}\mathbf{1} - (\boldsymbol{h} + \mathbf{\Sigma}_R)\end{bmatrix}^{-1},$$

with $\mathbf{h} = \boldsymbol{H}_{0,1,1}$ being the diagonal slice of the Hamiltonian. From this we can calculate required diagonal element $\boldsymbol{G}_{0,0}$ as

$$\begin{aligned}\boldsymbol{G}_{0,0} &= (\boldsymbol{A} - \boldsymbol{B}\boldsymbol{D}^{-1}\boldsymbol{C})^{-1},\\ \boldsymbol{A} &= E_{\mathrm{F}}\mathbf{1} - (\boldsymbol{h} + \mathbf{\Sigma}_L)\\ \boldsymbol{B} &= \boldsymbol{\tau}^\dagger\\ \boldsymbol{C} &= \boldsymbol{\tau}\\ \boldsymbol{D} &= E_{\mathrm{F}}\mathbf{1} - (\boldsymbol{h} + \mathbf{\Sigma}_R),\end{aligned} \quad (36)$$

which we found to be more stable than the direct calculation from Eq. (33).

The general expression described in this section can be used to compute the Green's function of translationally invariant devices like graphene ribbons, carbon nanotubes, quantum wires, straight channels, etc. Translational symmetry of the problem stated in Eq. (30) allows us to store just one row of the Green's function, hence the memory usage scales linearly as $(n + 1)L^2$, where L is the size of the $\boldsymbol{G}_{0,0}$ matrix and n is the number of off-diagonal elements to be computed. The standard approach requires n^2L^2 elements to be stored, therefore much larger systems can be stored with this method. The speed of the algorithm depends mostly on the time needed for computation of the self-energies, two $L \times L$ matrix inversions in Eq. (36), and n matrix-matrix multiplications defined by equations (34) and (36). Finally, in this case one can easily compute $\mathbf{\Psi}_{M_L}^{P}$ (20) and $\overleftarrow{\mathbf{\Psi}}_{M_{L'}}^{P(T)}$(21) matrices from pure propagation as in Eq. (32).

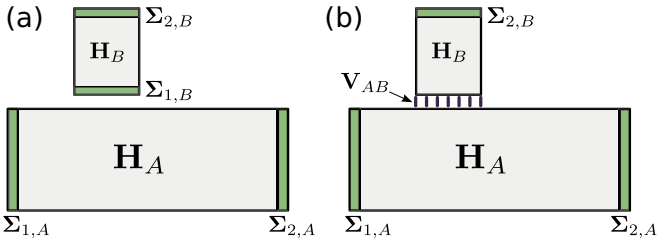

FIG. 2. (a) Schematics of two uncoupled infinite channels horizontal A and vertical B. (b) System B is glued to system A with coupling matrix $\mathbf{V}_{AB}$ which removes the self-energy term from the Hamiltonian B and connects proper sites of both systems.

C. Modular approach to compute Green's function

The result derived in the previous section can be used to construct efficiently more complicated devices built from translational invariant blocks connected with proper coupling matrix by using the Dyson equation, similarly as in Ref. [45,53]. As an example we consider a system created from two channels: a horizontal and a vertical one [see Fig. 2(a)]. Green's function of separated systems can be computed from Eqs. (34) and (35). The Hamiltonian and the Green's function of uncoupled systems can be written as

$$\mathbf{H}_0 = \begin{bmatrix}\boldsymbol{H}_A & \mathbf{0}\\ \mathbf{0} & \boldsymbol{H}_B\end{bmatrix}, \quad \mathbf{G}_0 = \begin{bmatrix}\boldsymbol{G}_A & \mathbf{0}\\ \mathbf{0} & \boldsymbol{G}_B\end{bmatrix},$$

with $\boldsymbol{H}_X = E_F\mathbf{1} - (\boldsymbol{H}_{0,X} + \Sigma_{1,X} + \Sigma_{2,X})$, with $\boldsymbol{H}_{0,X}$ being the Hamiltonian of a closed system.

We can glue both systems with Dyson equation

$$\mathbf{G} = \mathbf{G}_0 + \mathbf{G}_0\mathbf{V}_{AB}\mathbf{G}, \quad (37)$$

where the coupling matrix $\mathbf{V}_{AB}$ glues selected sites of system A and B with matrix τ_{AB} and removes the self-energy term in the lead 1 of systems B [see Fig. 2(b)]. This procedure creates the three terminal device. The $\mathbf{V}_{AB}$ matrix can be mathematically written as

$$\mathbf{V}_{AB} = \begin{bmatrix}\mathbf{0} & \tau_{AB}^\dagger\\ \tau_{AB} & \Sigma_{1,B}\end{bmatrix}.$$

Having $\mathbf{V}_{AB}$ and $\mathbf{G}_0$ one may compute selected elements of $\mathbf{G}$ using the standard approach which solves the Dyson equation (37).

Let us consider another example of two channels created from two different materials, e.g., ferromagnetic A and superconducting B channels or p-n junction as discussed in the next section [see Fig. 3(a)]. Similarly as previously, we can easily compute the Green's function of separated channels

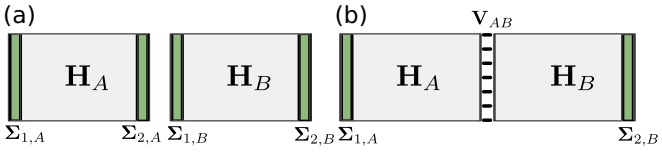

FIG. 3. (a) Schematic picture of two uncoupled infinite channels describing different materials. (b) After gluing with proper coupling matrix the systems form a quantum junction.

and then glue them together to form a quantum junction with proper coupling matrix which removes the self-energies in lead 2 of channel A and lead 1 of channel B [see Fig. 3(b)]

$$\mathbf{V}_{AB} = \begin{bmatrix} \Sigma_{2,A} & \tau_{AB}^{\dagger} \\ \tau_{AB} & \Sigma_{1,B} \end{bmatrix}. \tag{38}$$

V. APPLICATION TO GRAPHENE

Graphene and its transport properties [54] have been under an intense investigation for over a decade. The crystal structure with two nonequivalent triangular sublattices produces a gapless energy band structure with carriers that behave as massless Dirac fermions near the charge neutrality point. The presence of two sublattices and the resulting two nonequivalent Dirac points (K and K' valleys) forming a symmetric couple under the time inversion leads in particular to the suppression of the backscattering of chiral carriers by long-range potentials [55] and to half plateaux of conductance in the quantum Hall regime [56–59].

A. Current equilibration in graphene *p-n* junction

In graphene the regions of hole or electron conductivity are induced by external gates, with formation of the n-p junction in the intrinsic material of homogeneous chemical composition. The n-p junction is transparent for electrons incident normally [60] to the junction (Klein tunneling), and a strong angular dependence of the transfer probability was used for construction of the Fabry-Pérot interference in the n-p-n junctions [61,62]. However, in the quantum Hall regime, in high magnetic fields, the n-p junctions serve as waveguides for the charge currents [27,28]. The current confinement at the junction can be classically understood as due to the Lorentz force that acts in opposite directions for the carriers of the conduction and valence bands. The carriers move along the junction on snake orbits [63–67].

The values of conductance plateaux of the n-p junctions in the quantum Hall regime can be derived from the assumption of current equilibration, i.e., mixing of the modes at the contact between the edge and the n-p junction [27,68]. The mixing is a noncoherent process and its simulation requires an account taken for dephasing. One of the procedures [15] uses averaging the conductance through junction over N_{samp} different configurations of random on-site potential introduced on p-n interface, i.e., atoms which belong to the green areas in Fig. 4(a). We set the nearest neighbor carbon-carbon hopping energy to 2.7 eV. The potential energy in p region is tuned by external gate $\mathbf{V}_{\text{LG}}$. The number of carbon atoms in the lead cell (see green areas in Fig. 4) is set to 426 which gives a ribbon of width ∼450 Å for zigzag edge. The total number of

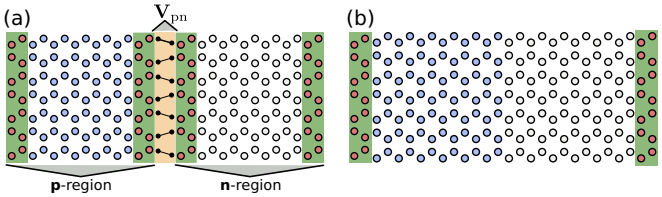

FIG. 4. (a) Sketch of two infinite systems which define p and n parts of the graphene p-n junction. Two systems are then glued with coupling matrix $\mathbf{V}_{\text{pn}}$. (b) The p-n junction after gluing process. The green areas denote the lead unit cells.

atoms in the whole structure is 17 466 with total length ∼50 Å. Note that for this case the size of the $\mathbf{G}_{\text{int}}$ is $2 \times 426 = 852$. The magnetic field is set to 67 T at which the quantum Hall effect appears. The on-site energy is uniformly distributed in range $[-W/2, W/2]$ with the disorder strength $W = 10$ eV. Additionally, for each configuration we choose randomly 105 of all interface atoms to be affected by on-site energy.

Green's function of the graphene p-n junction can be constructed by gluing two infinite systems together. The schematics of the gluing process is depicted in Fig. 4(a). Numerically, the Green's function of each separated system is calculated with efficient recursive formulas (34) and (35) and the coupling matrix $\mathbf{V}_{\text{pn}}$ defined in Eq. (38) removes the self-energy matrices and adds hoppings between carbon atoms at the p-n interface [see black segments in Fig. 4(a)]. Then the Green's function matrix $\mathbf{G}_{\text{int}}$ of atoms at the p-n interface can be computed directly from Dyson equation

$$\mathbf{G}_{\text{int}} = \left(\mathbf{1} - \mathbf{G}_{\text{pn}}^{0}\mathbf{V}_{\text{pn}}\right)^{-1}\mathbf{G}_{\text{pn}}^{0},$$

where

$$\mathbf{G}_{\text{int}} = \begin{pmatrix} \mathbf{G}_{\text{pp}} & \mathbf{G}_{\text{pn}} \\ \mathbf{G}_{\text{np}} & \mathbf{G}_{\text{nn}} \end{pmatrix},$$

$$\mathbf{G}_{\text{pn}}^{0} = \begin{pmatrix} \mathbf{G}_{\text{p}} & \mathbf{0} \\ \mathbf{0} & \mathbf{G}_{\text{n}} \end{pmatrix}.$$

For this configuration the method described above allows for a speedup by a factor of ∼50 in comparison to the standard WFM method [29,30]. The averaged conductance for $N_{\text{samp}} = 10\,000$ and a clean p-n junction is depicted in Figs. 5(a) and 5(b). This can be compared with Fig. 5(c) obtained from analytical model for fully equilibrated currents

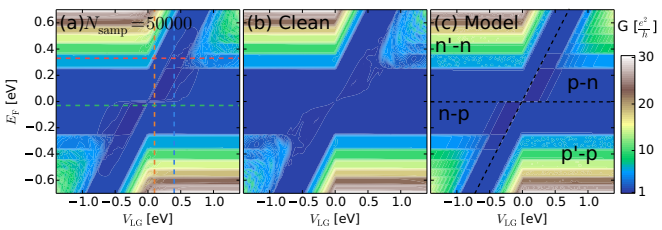

FIG. 5. (a) Averaged conductance as a function of Fermi level energy and potential energy $\mathbf{V}_{\text{LG}}$ in the p region obtained for $N_{\text{samp}} = 10\,000$ random configuration of on-site disorder at p-n junction interface. (b) Same as (a) but for clean junction (no averaging). (c) Analytical prediction adapted from Ref. [27].

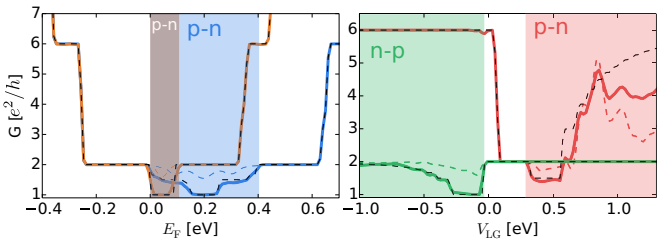

FIG. 6. The cross sections along vertical (a) and horizontal (b) lines in Fig. 5(a). The black dashed lines on each plot show the analytical prediction for fully equilibrated currents [Fig. 5(c)]. Thick color lines correspond to averaged conductance from Fig. 5(a). Dashed color lines correspond to the conductance of clean p-n junction from Fig. 5(b).

[27]. The letters in Fig. 5(c) denote the different working regimes.

For unipolar regions (n'-n and p'-p in Fig. 5) we obtain the same conductance values with or without averaging which agree with the analytical value of $G = \frac{e^2}{h}\min(\nu_1,\nu_2)$ [27], where ν_1 and ν_2 are the Landau level filling factors $(\nu_1,\nu_2 = \pm 2, \pm 6, \pm 10)$ for the two parts of the gated ribbon. In these conditions the conductance equals the maximal number of conducting modes for the edge transport which resists backscattering. For the parameters corresponding to the n-p junction the conductance plateau is given by [27] $G = \frac{e^2}{h}\frac{|\nu_1||\nu_2|}{|\nu_1|+|\nu_2|} = 1, 3/2, 3, \ldots$. For the adopted parameters of the random potential only the first two lowest values are resolved as plateaux (see Fig. 6). The applied method [15] requires optimization of the random disorder parameters for each subsequent conductance plateaux. Note that also in the experiment the conductance plateaux at the n-p charge configuration are less precisely defined than in the unipolar regime—see left-hand side of Figs. 3(c) and 3(d) of Ref. [28].

B. Magnetic focusing in graphene

The mean free path of the carriers in graphene reaches several microns at low temperatures. When an external magnetic field is applied perpendicular to the graphene plane the electrons move on cyclotron orbits that can be resolved with the scanning gate microscopy technique (SGM) [23,24,69]. In the SGM measurements the conductance maps are gathered as functions of the position of the atomic force microscope tip that acts as a floating gate. The numerical method described above is a high-performance tool for evaluation of the conductance maps since (i) the potential of the tip is short range due to screening the potential of the floating gate by the electron gas, and (ii) for evaluation of the conductance map one needs to solve the quantum scattering problem for each location of the tip.

The considered device is built from a large electron reservoir A (see Fig. 7) connected to two smaller leads, the source L_1 and the drain L_2 lead (similarly as in the example in Sec. IV C). The Green's function of system A is calculated from recursive formulas (34) and (35) and the Green's functions at the interface of attached leads L_1 and L_2 are computed with the knitting method [49]. We define the unperturbed system as the one constructed from three areas:

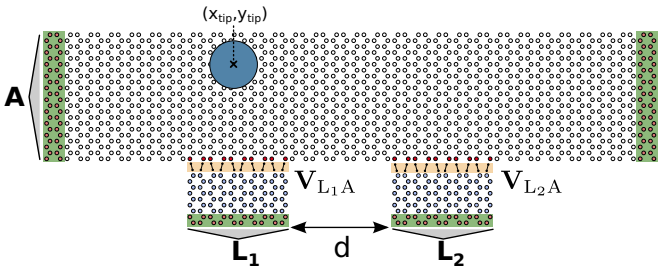

FIG. 7. The sketch of the magnetic focusing device. The large reservoir A is built from 191 000 atoms and is connected with two smaller vertical leads $L_{1/2}$ with coupling matrices $\mathbf{V}_{mL_{1/2},A}$ separated by distance $d = 320$ Å. The blue disk shows the SGM tip influence radius. Only the atoms below the blue area are affected by the SGM potential.

A and the leads $L_{1/2}$ but without mutual coupling between them. Then the Green's function is constructed from the Dyson equation. However, in that case the disorder matrix $\mathbf{V}_{PP}$ results from (a) the SGM tip potential which is modeled as a smooth disk of radius $d_{tip} = 13$ Å with expression

$$V_{tip}(\mathbf{r}) = U_{tip} e^{-(\frac{|\mathbf{r}-\mathbf{r}_{tip}|}{d_{tip}})^8},$$

where the center of the tip is located at $\mathbf{r}_{tip}$ and $U_{tip} = 4$ eV and (b) the coupling between leads $L_{1/2}$ interface sites and A atoms (see black segments in Fig. 7). For each position of the tip we list all the atoms for which condition $V_{tip}(\mathbf{r}_{atom}) > 10^{-3}$ eV is satisfied, resulting in about 300 atoms on average. The coupling between $L_{1/2}$ and A is introduced at 120 atoms for both leads. Hence, the full coupling matrix $\mathbf{V}_{PP}$ and the reduced Green's function matrices are of size about 420×420. In our simulations the A system is build from 191 000 carbon atoms (with 764 atoms in lead unit cell) and the small leads $L_{1/2}$ contains 2970 atoms (with 60 atoms in lead cell) separately. The distance d between the vertical leads is set to 320 Å. The width and the length of the A ribbon are 470 Å and 1060 Å, respectively. The Fermi energy E_F is set to 0.5 eV. For this set of parameters we obtain the speedup $\sim$15 in comparison to the standard method.

In Fig. 8 we show the conductance between the source and drain leads as a function of magnetic field amplitude. The conductance is calculated with a standard method and the higher conductance means a higher probability that the electron will get from lead L_1 to L_2. Three peaks are clearly visible for $B = 27, 54, 81$ T.

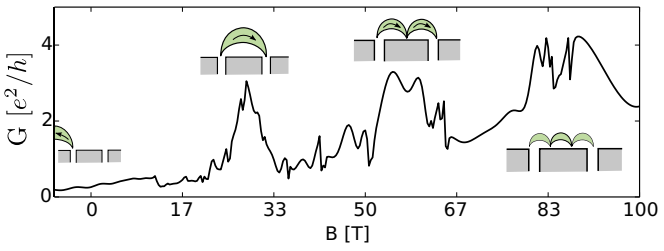

FIG. 8. Conductance between vertical leads as a function of magnetic field amplitude. The insets indicate the trajectories behind the conductance peaks.

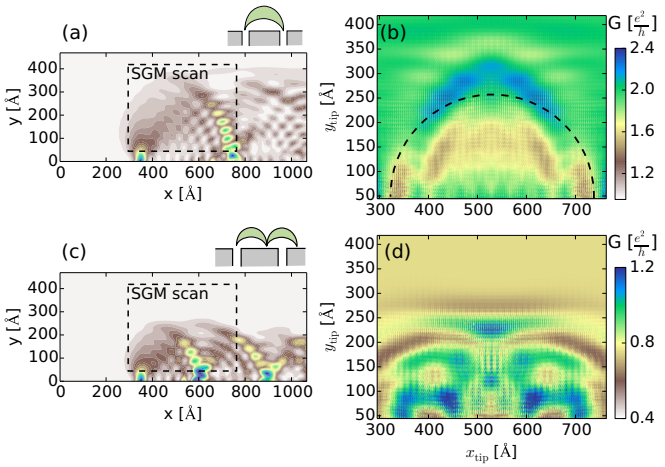

FIG. 9. (a) The scattering electron density for electron incoming from lead $\mathbf{L}_1$ at $B = 27$ T. The black dashed line shows the SGM scan area. (b) Simulated SGM image for the case from (a). Dashed arc corresponds to the classical cyclotron orbit. (c),(d) same as (a),(b) but obtained for $B = 40$ T. The electron densities of (a),(c) are calculated from direct solution of the scattering problem and the SGM map with the method introduced in this paper.

For $E_F = 0.5$ eV and $V_F = 10^6$ m/s, the electron density is $n = \frac{E_F^2}{\pi(\hbar V_F)^2} = 18.31 \times 10^{12}/\text{cm}^2$, and the dynamical electron mass [23] equals $m^* = \hbar\sqrt{\pi n}/V_F = 0.087 m_0$. Then, the cyclotron diameter is equal to $d_c = 2m^* V_F/eB = \frac{1000\text{nmT}}{B}$. For the values of B corresponding to the first conductance peak the cyclotron radius is equal to 37.5 nm, which agrees well with the distance between the axis of the vertical leads L_1 and L_2 that equals 38 nm. We conclude that the peaks correspond to integer multiples of cyclotron diameters. For magnetic fields $B < 0$ the current is deflected towards the left and hence the current quickly drops to zero.

In Fig. 9(a) we show the scattering electron density obtained for $B = 27.5$ T (i.e., the first peak of the conductance in Fig. 8) calculated as $\sum_m |\Psi_{l_1,m}|^2$ for the unperturbed system by a direct solution of scattering problem using standard method WFM, i.e., obtained for fully glued system. The skipping orbits are clearly seen in the density plot. In Fig. 9(b) we show the SGM image calculated with the method of the present paper which can be compared with the experimental results given in Fig. 3(b) of Ref. [23]. Note, in Fig. 9(b) the scattering problem needs to be recalculated for each position of the SGM tip. The theoretical result of Fig. 9(a) reproduces the reduced value of conductance when the tip is above the cyclotron orbit and thus prevents the electrons from passing from L_1 to L_2. Moreover, the present result reproduces the region of increased conductance when the tip is above the cyclotron orbit, and when it scatters the electrons to L_2, and next a ring of reduced conductance, exactly as observed in Fig. 3(b) of Ref. [23]. To our knowledge the present result is the first simulation of the magnetic focusing experiment of Ref. [23] that is based on the solution of the quantum scattering problem (Ref. [23] used a classical picture for the interpretation). For completeness in Figs. 9(c) and 9(d) we show the electron density at a minimum of the conductance ($B = 40$ T) with the simulated SGM image. Formation of a skipping orbit is observed, but with the size that does not coincide with the distance between the feeding and drain contacts.

VI. CONCLUSIONS

To summarize, we have shown that by projecting the time reversed scattering wave function onto Lippmann-Schwinger equation we may significantly reduce the number of Green's function elements needed for computation of the scattering matrix of arbitrary TB systems in the ballistic transport approximation.

We have studied the weak perturbation regime for which we have shown that the first correction to the conductance does not depend on the Green's function of the unperturbed system which resembles the existing formulas obtained from analytical models. In the case of the one-dimensional wire with delta-like impurity we have shown that the diagonal element of the Green's function (i.e., local density of states) at the perturbation site can be extracted from conductance versus impurity strength characteristic. Additionally, we have discussed the possible applications of our method for (a) current equilibration at the graphene p-n junction interface, obtaining fractional conductance steps similar to those found in the experiment [28], (b) simulation of imaging of the cyclotron orbits in magnetic focusing experiment with good agreement with Ref. [23]. For both cases we have obtained significant speedup in comparison to the standard wave function matching method.

ACKNOWLEDGMENTS

This work was supported by the National Science Centre according to decision DEC-2015/17/B/ST3/01161. The first and second authors acknowledge the scholarship of Krakow Smoluchowski Scientific Consortium from the funding for National Leading Reserch Centre by Ministry of Science and Higher Education (Poland) and ETIUDA doctotal stipends of the National Science Centre (NCN) according to decisions DEC-2015/16/T/ST3/00310, and DEC-2015/16/T/ST3/00264, respectively. The authors are grateful to Xavier Waintal and Christoph Groth for valuable and stimulating discussion. The calculations were performed at PL-Grid Infrastructure.

APPENDIX

Note on stable calculation of scattering amplitudes

After solution of the scattering problem one has to calculate scattering amplitudes from Eqs. (6) and (7) which involves inversion of possibly ill-conditioned $\boldsymbol{U}_{l,-}$ matrix [34]. However, one may note that we do not need to calculate the whole $\mathbf{t}^{l'}_{l,m}$ and $\mathbf{r}^{l'}_{l,m}$ vectors, but only those elements which correspond to the propagating modes, i.e., $\mathbf{t}^{l'}_{l,m} = (t^{l',1}_{l,m}, \ldots, t^{l',M}_{l,m}, t^{l',M+1}_{l,m}, \ldots, t^{l',N_{L'}}_{l,m})$, with M being the number of propagating modes in the lead l'. In order to calculate the first M elements of vector $\mathbf{t}^{l'}_{l,m}$ (the procedure for $\mathbf{r}^{l'}_{l,m}$ is the same) we apply QL factorization of $\boldsymbol{U}_{l',-}$ matrix

$$\boldsymbol{U}_{l',-} = \boldsymbol{Q}\boldsymbol{L}, \tag{A1}$$

with $\boldsymbol{Q}$ being an unitary matrix, and $\boldsymbol{L}$ a lower triangular matrix. The QL factorization can be done even if $\boldsymbol{U}_{l',-}$ is noninvertible. Now, we can use the fact that $\mathbf{Q}$ can be easily inverted ($\mathbf{Q}^{-1} = \mathbf{Q}^{\dagger}$) and $\mathbf{L}$ is a triangular matrix to solve Eq. (6). However, there is no reason for the first $M \times M$ top-left block of the $\boldsymbol{L}$ matrix to be well conditioned, and the algorithm may lead to numerical errors. To avoid this problem we have found that performing QL factorization of transformed matrix

$$\boldsymbol{U}^{\dagger}_{\mathrm{SVD}}\boldsymbol{U}_{l',-} = \boldsymbol{Q}'\boldsymbol{L}', \tag{A2}$$

instead of (A1), leads to well ordered triangular matrix $\boldsymbol{L}'$, where $\boldsymbol{U}_{l',-} = \boldsymbol{U}_{\mathrm{SVD}}\mathbf{S}_{\mathrm{SVD}}\boldsymbol{V}^{\dagger}_{\mathrm{SVD}}$ is the definition of SVD [34] and $\mathbf{S}_{\mathrm{SVD}}$ is a diagonal matrix, whose diagonal elements $S_{\mathrm{SVD},k}$ are the singular values which are positive, real, and ordered in the descending order. From Eq. (A2) we have $\boldsymbol{U}_{l',-} = \boldsymbol{U}_{\mathrm{SVD}}\boldsymbol{Q}'\boldsymbol{L}'$ which we put to Eq. (6) to get

$$\boldsymbol{L}'\mathbf{t}^{l'}_{l,m} = \boldsymbol{Q}'^{\dagger}\boldsymbol{U}^{\dagger}_{\mathrm{SVD}}\boldsymbol{\Psi}^{L'}_{l,m} \equiv \boldsymbol{d}_m.$$

Since $\boldsymbol{L}'$ is a lower triangular matrix we may easily calculate first Mth elements with simple recursion without explicit inversion of the full $\boldsymbol{L}'$ matrix

$$t^{l',k}_{l,m} = \left(d_{m,k} - \sum_{i=1}^{k-1} L'_{k,i}t^{l',i}_{l,m}\right) \Big/ L'_{k,k}.$$

We find this approach to be more accurate in comparison to direct inversion of $\boldsymbol{U}_{l',-}$ which in general can be noninvertible. The reason of the improved stability of Eq. (A2) comes from the property of the SVD which order the singular values of the $\boldsymbol{U}_{l',-}$ matrix in descending order, hence the first M rows and columns of $\boldsymbol{U}^{\dagger}_{\mathrm{SVD}}\boldsymbol{U}_{l',-} = S_{\mathrm{SVD}}\boldsymbol{V}^{\dagger}_{\mathrm{SVD}}$ matrix contain a contribution of nonsingular values leading to a more stable algorithm.

[1] S. Datta, *Electronic Transport in Mesoscopic Systems* (Cambridge University Press, Cambridge, 1995).
[2] H. Sellier, B. Hackens, M. G. Pala, F. Martins, S. Baltazar, X. Wallart, L. Desplanque, V. Bayot, and S. Huant, Semicond. Sci. Technol. **26**, 064008 (2011).
[3] D. K. Ferry, A. M. Burke, R. Akis, R. Brunner, T. E. Day, R. Meisels, F. Kuchar, J. P. Bird, and B. R. Bennett, Sem. Sci. Tech. **26**, 043001 (2011).
[4] M. A. Topinka, B. J. LeRoy, S. E. J. Shaw, E. J. Heller, R. M. Westervelt, K. D. Maranowski, and A. C. Gossard, Science **289**, 2323 (2000).
[5] M. A. Topinka, B. J. LeRoy, R. M. Westervelt, S. E. J. Shaw, R. Fleischmann, E. J. Heller, K. D. Maranowski, and A. C. Gossard, Nature (London) **410**, 183 (2001).
[6] A. A. Kozikov, R. Steinacher, C. Rössler, T. Ihn, K. Ensslin, C. Reichl, and W. Wegscheider, Nano Lett. **15**, 7994 (2015).
[7] M. P. Jura, M. A. Topinka, L. Urban, A. Yazdani, H. Shtrikman, L. N. Pfeiffer, K. W. West, and D. Goldhaber-Gordon, Nat. Phys. **3**, 841 (2007).
[8] M. P. Jura, M. A. Topinka, M. Grobis, L. N. Pfeiffer, K. W. West, and D. Goldhaber-Gordon, Phys. Rev. B **80**, 041303 (2009).
[9] B. L. Altshuler, D. Khmel'nitzkii, A. I. Larkin, and P. A. Lee, Phys. Rev. B **22**, 5142 (1980).
[10] P. D. Dresselhaus, C. M. A. Papavassiliou, R. G. Wheeler, and R. N. Sacks, Phys. Rev. Lett. **68**, 106 (1992).
[11] W. Knap, C. Skierbiszewski, A. Zduniak, E. Litwin-Staszewska, D. Bertho, F. Kobbi, J. L. Robert, G. E. Pikus, F. G. Pikus, S. V. Iordanskii, V. Mosser, K. Zekentes, and Y. B. Lyanda-Geller, Phys. Rev. B **53**, 3912 (1996).
[12] T. Hassenkam, S. Pedersen, K. Baklanov, A. Kristensen, C. B. Sorensen, P. E. Lindelof, F. G. Pikus, and G. E. Pikus, Phys. Rev. B **55**, 9298 (1997).
[13] A. F. Morpurgo and F. Guinea, Phys. Rev. Lett. **97**, 196804 (2006).
[14] M. G. Pala and G. Iannaccone, Phys. Rev. B **69**, 235304 (2004).
[15] W. Long, Q.-f. Sun, and J. Wang, Phys. Rev. Lett. **101**, 166806 (2008).
[16] F. Libisch, S. Rotter, and J. Burgdörfer, New J. Phys. **14**, 123006 (2012).
[17] B. A. Lippmann and J. Schwinger, Phys. Rev. **79**, 469 (1950).
[18] R. A. Jalabert, W. Szewc, S. Tomsovic, and D. Weinmann, Phys. Rev. Lett. **105**, 166802 (2010).
[19] C. Gorini, R. A. Jalabert, W. Szewc, S. Tomsovic, and D. Weinmann, Phys. Rev. B **88**, 035406 (2013).
[20] J. Horáček and T. Sasakawa, Phys. Rev. A **28**, 2151 (1983).
[21] L. K. Castelano, G.-Q. Hai, and M.-T. Lee, Phys. Rev. B **76**, 165306 (2007).
[22] K. E. Aidala, R. E. Parrott, T. Kramer, E. J. Heller, R. M. Westervelt, M. P. Hanson, and A. C. Gossard, Nat. Phys. **3**, 464 (2007).
[23] S. Bhandari, G.-H. Lee, A. Klales, K. Watanabe, T. Taniguchi, E. Heller, P. Kim, and R. M. Westervelt, Nano Lett. **16**, 1690 (2016).
[24] T. Taychatanapat, K. Watanabe, T. Taniguchi, and P. Jarillo-Herrero, Nat. Phys. **9**, 225 (2013).
[25] B. Özyilmaz, P. Jarillo-Herrero, D. Efetov, D. A. Abanin, L. S. Levitov, and P. Kim, Phys. Rev. Lett. **99**, 166804 (2007).
[26] S. Nakaharai, J. R. Williams, and C. M. Marcus, Phys. Rev. Lett. **107**, 036602 (2011).
[27] D. A. Abanin and L. S. Levitov, Science **317**, 641 (2007).
[28] J. R. Williams, L. DiCarlo, and C. M. Marcus, Science **317**, 638 (2007).
[29] H. H. B. Sørensen, P. C. Hansen, D. E. Petersen, S. Skelboe, and K. Stokbro, Phys. Rev. B **79**, 205322 (2009).
[30] M. Zwierzycki, P. A. Khomyakov, A. A. Starikov, K. Xia, M. Talanana, P. X. Xu, V. M. Karpan, I. Marushchenko, I. Turek, G. E. W. Bauer, G. Brocks, and P. J. Kelly, Phys. Stat. Sol. **245**, 623 (2008).
[31] K. Xia, M. Zwierzycki, M. Talanana, P. J. Kelly, and G. E. W. Bauer, Phys. Rev. B **73**, 064420 (2006).
[32] M. Leng and C. S. Lent, J. Appl. Phys. **76**, 2240 (1994).
[33] C. S. Lent and D. J. Kirkner, J. Appl. Phys. **67**, 6353 (1990).
[34] I. Rungger and S. Sanvito, Phys. Rev. B **78**, 035407 (2008).
[35] M. Wimmer (Universität Regensburg, Regensburg, 2009).

[36] J. Cerdá, M. A. Van Hove, P. Sautet, and M. Salmeron, Phys. Rev. B **56**, 15885 (1997).
[37] S. Kramer, Phys. Rev. B **88**, 125308 (2013).
[38] A. C. Neto, V. Kotov, J. Nilsson, V. Pereira, N. Peres, and B. Uchoa, Solid State Commun. **149**, 1094 (2009).
[39] S. Irmer, T. Frank, S. Putz, M. Gmitra, D. Kochan, and J. Fabian, Phys. Rev. B **91**, 115141 (2015).
[40] M. Gmitra, D. Kochan, and J. Fabian, Phys. Rev. Lett. **110**, 246602 (2013).
[41] J. W. Demmel, S. C. Eisenstat, J. R. Gilbert, X. S. Li, and J. W. H. Liu, SIAM J. Matrix Anal. Appl. **20**, 720 (1999).
[42] O. Schenk, A. Wächter, and M. Hagemann, Comput. Optim. Appl. **36**, 321 (2007).
[43] G. Metalidis and P. Bruno, Phys. Rev. B **72**, 235304 (2005).
[44] S. Sanvito, C. J. Lambert, J. H. Jefferson, and A. M. Bratkovsky, Phys. Rev. B **59**, 11936 (1999).
[45] S. Rotter, B. Weingartner, N. Rohringer, and J. Burgdörfer, Phys. Rev. B **68**, 165302 (2003).
[46] D. Guan, U. Ravaioli, R. W. Giannetta, M. Hannan, I. Adesida, and M. R. Melloch, Phys. Rev. B **67**, 205328 (2003).
[47] M. Settnes, S. R. Power, J. Lin, D. H. Petersen, and A.-P. Jauho, Phys. Rev. B **91**, 125408 (2015).
[48] G. Thorgilsson, G. Viktorsson, and S. Erlingsson, J. Comput. Phys. **261**, 256 (2014).
[49] K. Kazymyrenko and X. Waintal, Phys. Rev. B **77**, 115119 (2008).
[50] U. Hetmaniuk, Y. Zhao, and M. Anantram, Int. J. Numer. Meth. Eng. **95**, 587 (2013).
[51] K. Kolasiński, our simple Knitting algorithm source code can be found at https://gitlab.com/kmkolasinski/knitinv.
[52] P. A. Khomyakov, G. Brocks, V. Karpan, M. Zwierzycki, and P. J. Kelly, Phys. Rev. B **72**, 035450 (2005).
[53] F. Sols, M. Macucci, U. Ravaioli, and K. Hess, J. Appl. Phys. **66**, 3892 (1989).
[54] A. H. Castro Neto, F. Guinea, N. M. R. Peres, K. S. Novoselov, and A. K. Geim, Rev. Mod. Phys. **81**, 109 (2009).
[55] T. Ando, J. Phys. Soc. Jpn. **74**, 777 (2005).
[56] K. S. Novoselov, Z. Jiang, Y. Zhang, S. V. Morozov, H. L. Stormer, U. Zeitler, J. C. Maan, G. S. Boebinger, P. Kim, and A. K. Geim, Science **315**, 1379 (2007).
[57] K. S. Novoselov, A. K. Geim, S. V. Morozov, D. Jiang, M. I. Katsnelson, I. V. Grigorieva, S. V. Dubonos, and A. A. Firsov, Nature (London) **438**, 197 (2005).
[58] Y. Zhang, Y.-W. Tan, H. L. Stormer, and P. Kim, Nature (London) **438**, 201 (2005).
[59] V. P. Gusynin and S. G. Sharapov, Phys. Rev. Lett. **95**, 146801 (2005).
[60] M. I. Katsnelson, K. S. Novoselov, and A. K. Geim, Nat. Phys. **2**, 620 (2006).
[61] A. V. Shytov, M. S. Rudner, and L. S. Levitov, Phys. Rev. Lett. **101**, 156804 (2008).
[62] A. F. Young and P. Kim, Nat. Phys. **5**, 222 (2009).
[63] P. Carmier, C. Lewenkopf, and D. Ullmo, Phys. Rev. B **81**, 241406 (2010).
[64] J. R. Williams and C. M. Marcus, Phys. Rev. Lett. **107**, 046602 (2011).
[65] L. Oroszlány, P. Rakyta, A. Kormányos, C. J. Lambert, and J. Cserti, Phys. Rev. B **77**, 081403 (2008).
[66] T. K. Ghosh, A. De Martino, W. Häusler, L. Dell'Anna, and R. Egger, Phys. Rev. B **77**, 081404 (2008).
[67] M. Zarenia, J. M. Pereira, F. M. Peeters, and G. A. Farias, Phys. Rev. B **87**, 035426 (2013).
[68] N. Kumada, F. D. Parmentier, H. Hibino, D. C. Glattli, and P. Roulleau, Nat. Commun. **6**, 8068 (2015).
[69] S. Morikawa, Z. Dou, S.-W. Wang, C. G. Smith, K. Watanabe, T. Taniguchi, S. Masubuchi, T. Machida, and M. R. Connolly, Appl. Phys. Lett. **107**, 243102 (2015).